



Published in final edited form as:

J Biomech. 2017 December 08; 65: 145–153. doi:10.1016/j.jbiomech.2017.10.018.

Examining tissue composition, whole-bone morphology and mechanical behavior of *Gorab*^{Prx1} mice tibiae: a mouse model of premature aging

Haisheng Yang^{a,b}, Laia Albiol^c, Wing-Lee Chan^d, Dag Wulsten^c, Anne Seliger^c, Michael Thelen^d, Tobias Thiele^c, Lyudmila Spevak^e, Adele Boskey^e, Uwe Kornak^{d,f,g}, Sara Checa^c, and Bettina M. Willie^{b,c,*}

^aDepartment of Biomedical Engineering, College of Life Science and Bioengineering, Beijing University of Technology, Beijing, China

^bResearch Centre, Shriners Hospital for Children-Canada, Department of Pediatric Surgery, McGill University, Canada

^cJulius Wolff Institute, Charité-Universitätsmedizin Berlin, Berlin, Germany

^dInstitute for Medical Genetics and Human Genetics, Charité-Universitätsmedizin Berlin, Germany

^eHospital for Special Surgery, New York, USA

^fBerlin-Brandenburg Center for Regenerative Therapies, Charité-Universitätsmedizin Berlin, Germany

^gMax Planck Institute for Molecular Genetics, Germany

Abstract

Gerodermia osteodysplastica (GO) is a segmental progeroid disorder caused by loss-of-function mutations in the *GORAB* gene, associated with early onset osteoporosis and bone fragility. A conditional mouse model of GO (*Gorab*^{Prx1}) was generated in which the *Gorab* gene was deleted in long bones. We examined the biomechanical/functional relevance of the *Gorab*^{Prx1} mutants as a premature aging model by characterizing bone composition, tissue-level strains, and whole-bone morphology and mechanical properties of the tibia. MicroCT imaging showed that *Gorab*^{Prx1} tibiae had an increased anterior convex curvature and decreased cortical cross-sectional area, cortical thickness and moments of inertia, compared to littermate control (LC) tibiae. Fourier transform infrared imaging (FTIRI) indicated a 34% decrease in mineral/matrix ratio and a 27% increase in acid phosphate content in the posterior metaphyseal cortex of the *Gorab*^{Prx1} tibiae

*Contact information: Bettina Willie, Shriners Hospitals for Children-Canada, 1003 Decarie Blvd, Montreal, H4A 0A9, Canada, Phone: 514-282-7156, bwillie@shriners.mcgill.ca.

Conflict of Interest

The authors have no conflict of interest.

Publisher's Disclaimer: This is a PDF file of an unedited manuscript that has been accepted for publication. As a service to our customers we are providing this early version of the manuscript. The manuscript will undergo copyediting, typesetting, and review of the resulting proof before it is published in its final citable form. Please note that during the production process errors may be discovered which could affect the content, and all legal disclaimers that apply to the journal pertain.

($p < 0.05$), suggesting delayed mineralization. *In vivo* strain gauge measurement and finite element analysis showed ~two times higher tissue-level strains within the *Gorab*^{Prx1} tibiae relative to LC tibiae when subjected to axial compressive loads of the same magnitude. Three-point bending tests suggested that *Gorab*^{Prx1} tibiae were weaker and more brittle, as indicated by decreasing whole-bone strength (46%), stiffness (55%), work-to-fracture (61%) and post-yield displacement (47%). Many of these morphological and biomechanical characteristics of the *Gorab*^{Prx1} tibia recapitulated changes in other animal models of skeletal aging. Future studies are necessary to confirm how our observations might guide the way to a better understanding and treatment of GO.

Keywords

premature aging; osteoporosis; finite element analysis; bone composition; bone strength

1. Introduction

Geroderma osteodysplastica (GO, MIM#231070) is a hereditary segmental progeroid disorder (Al-Gazali et al., 2001; Hennies et al., 2008; Nanda et al., 2008; Rajab et al., 2008), one of the few monogenic disorders other than osteogenesis imperfecta that has pronounced osteoporosis and fractures already in childhood (Hunter, 1988; Lisker et al., 1979; Nanda et al., 2008). Individuals with GO also have a prematurely aged appearance with wrinkled skin and generalized connective tissue weakness (Al-Bughaili et al., 2017). GO is caused by loss-of-function mutations in GORAB (also named SCYL1-binding protein 1 or NTKL-binding protein 1), which is highly expressed in skin and bone (Hennies et al., 2008). The protein is probably involved in intra-Golgi trafficking processes (Egerer et al., 2015).

Recently, a mouse model of GO (*Gorab*^{Prx1}) has been developed by our group (Steiner et al., 2015), wherein *Gorab* is conditionally inactivated in the limb bud mesenchyme by crossing *Gorab*^{fllox} with Prx1-cre mice (Logan et al., 2002). The *Gorab*^{Prx1} mice showed mild growth retardation, a reduction of trabecular and cortical bone volume, and mineralization defects (Steiner et al., 2015). Furthermore, it has been demonstrated that loss of *Gorab* impairs proteoglycan synthesis leading to bone fragility through collagen disorganization, TGF-beta upregulation, and impaired osteoblast lineage differentiation, which may explain the pathomechanism of GO (Steiner et al., 2015). TGF-beta upregulation has also been implicated in two other disorders that are associated with osteoporosis or osteopenia, osteogenesis imperfecta (Glorieux and Moffatt, 2013) and Marfan syndrome (Nistala et al., 2010), respectively. Despite these insights into the molecular mechanisms of GO, bone fragility-related factors, including tissue material properties, whole-bone morphology and mechanical behavior of *Gorab*^{Prx1} bones have not been examined. Studying the early onset skeletal deterioration observed in *Gorab*^{Prx1} mice may provide insights into bone fragility associated with GO and help elucidate mechanisms underlying chronological skeletal aging (Jilka, 2013). Therefore, we examined the biomechanical/functional relevance of the *Gorab*^{Prx1} mouse model. Our objective was to characterize tissue composition, whole-bone morphology and mechanical behavior of the tibiae from *Gorab*^{Prx1} mice compared with littermate controls (LCs).

2. Materials and Methods

2.1 Animals

The study included 10–12 week-old female *Gorab*^{Prx1} mice and homozygous conditional *Gorab*^{fllox} mice without the cre allele from the same generation as LCs. The *Gorab*^{Prx1} mice were generated by crossing *Gorab*^{fllox} with Prx1-cre mice (Logan et al., 2002) to conditionally inactivate *Gorab* expression in limb bud mesenchyme (Steiner et al., 2015). Animals were backcrossed > 6 times with C57BL/6 mice. All procedures were approved by the local animal welfare legal authority (LaGeSo; Berlin, Germany; G0213/12).

2.2 In vivo tibial strain measurements

In vivo strain measurements were performed on the medial surface of the tibial midshaft in living 10 week-old LC and *Gorab*^{Prx1} mice to determine the relationship between applied tibial compressive loads and bone tissue deformation (n=5/genotype). While the mouse was anesthetized, an incision was made over the medial surface of the tibia and a uniaxial strain gauge (EA-06-015LA-120, Micromeritics, NC) mounted on the antero-medial surface of the tibial midshaft aligned with the bone's long axis. A range of dynamic compressive loads (peak loads ranging from –2 to –12 N) was applied through the knee and ankle joints, using an *in vivo* loading device (Testbench ElectroForce LM1, TA Instruments, DE) mounted with custom-designed fixtures (Fig. 1), recording load and strain measurements simultaneously. Measurements were performed for both left and right tibiae. Mice were euthanized following loading, while still under anesthesia. Axial rigidity, previously referred to by others as “*in vivo stiffness*” (Main et al., 2010), was calculated as the change in load over the change in strain and averaged for all load levels (–2, –4, –6, –8, –10, –12 N) to obtain a mean axial rigidity value for each tibia, from which the mean gauge-measured strain of the tibia can be calculated at a given load magnitude. The axial rigidity or the relationship between the axial compressive load and the strain generated at the gauge site is important since tissue level strain regulates bone growth and remodeling (Main et al., 2010).

2.3 Diaphyseal and metaphyseal geometric measurements

In an additional group of 10 week-old mice (n=8 *Gorab*^{Prx1}, n=10 LC) geometric measures were performed at two representative tibial regions (midshaft and proximal metaphysis) following microcomputed tomography (microCT; isotropic voxel size of 10.5 μm; vivaCT 40, Scanco Medical, Switzerland; 55 kVp, 145 μA, 600 ms integration time, no frame averaging). There were originally 10 *Gorab*^{Prx1} mice, but two mice died while under anesthesia during *in vivo* microCT scanning and therefore were excluded from the study. The proximal metaphyseal volume of interest (VOI) started 100 μm below the distal-most point of the growth plate and extended distally 10% of the tibial length (Willie et al., 2013; Yang et al., 2017). The cancellous and cortical bone in the metaphyseal VOI were segmented manually in the scans and analyzed separately. The cortical midshaft VOI was centered at the midpoint of the tibia and extended 5% of the tibial length (Willie et al., 2013; Yang et al., 2017). A threshold of 671 mg HA/ccm was used to segment both diaphyseal and metaphyseal cortical bone. A threshold of 450 mg HA/ccm was used to segment metaphyseal cancellous bone.

2.4 Characterization of tissue-level strains within the entire tibia

MicroCT-based finite element (FE) simulation was performed mimicking the *in vivo* tibial strain gauging experiment to determine tissue-level strains within the entire tibia. The FE approach used in this study had been developed and validated in C57BL/6 mice across a broad range of ages (10, 26, and 78 week old; (Razi et al., 2015; Yang et al., 2014)). To acquire whole bone geometry, *ex vivo* microCT (10 μm resolution) was performed on the entire tibiae that were strain-gauged *in vivo* (n=3 representative tibiae/genotype). Tibial FE models with tetrahedral elements were created following segmentation and bone surface extraction using Amira software (Zuse Institute, Berlin, Germany) (Razi et al., 2015). Homogeneous elastic material properties (Young's modulus of 13.8 GPa; (Razi et al., 2015)) were used for both LC and *Gorab*^{Prx1} FE models. Additionally, to estimate the influence of tissue heterogeneity on strain distributions, heterogeneous FE models of one representative bone per genotype were created and their strain predictions were compared with homogeneous models of the same bones. The heterogeneous modeling approach has been described in detail elsewhere (Razi et al., 2015; Albiol et al., 2017). Briefly, element-specific Young's modulus values were assigned to the FE models based on spatial distribution of the attenuation coefficient (μ) in the microCT scans. The Young's modulus (E) was calculated with a power-law equation $E = (\mu/\mu_{\text{max}})^{1.5} \times 17 \text{ GPa}$, where μ_{max} is the maximum attenuation coefficient in the whole-bone microCT scans.

Loading was applied in a direction representing the trajectory in which the actuator moves (Fig. 1; (Razi et al., 2015; Willie et al., 2013)). The compressive load was applied through a contact surface on the knee side, replicating the tibio-femoral contact areas. On the ankle side, the talus-tibialis contact surface nodes were constrained allowing displacement in antero-posterior direction and rotation around the medio-lateral axis. The same load level of -5 N was used for both LC and *Gorab*^{Prx1} models to compare their tissue-level strains; this load level was chosen because it induced ~1200 $\mu\epsilon$ at the tibial midshaft in *Gorab*^{Prx1} mice based on our *in vivo* strain gauge measures. This strain level has been shown to be osteogenic and is approximately 2–3 times the strain level engendered in C57Bl/6 mice during walking (De Souza et al., 2005; Sugiyama et al., 2012). Linear elastic FE analyses were performed (Abaqus, Dassault Systemés Simulia, MA). The strain at the gauge site in the model was calculated and compared with experimental measures above. The tibia was equally divided into 20 regions along its longitudinal direction. Compressive (minimum principal) and tensile (maximum principal) strains in each region were compared between LC and *Gorab*^{Prx1} mice.

2.5 Characterization of whole-bone morphology of the tibia

Radii of longitudinal curvature of the whole tibia were measured in anterior-posterior and medial-lateral directions based on reconstructed 3D tibial models above. Tibial axis was determined by a straight line connecting the centroids of the proximal and distal ends (regions) of the tibia (Galea et al., 2015; Main et al., 2010). In each of the 20 regions along the tibial length, the centroid of the bone section was identified, and then the anterior-posterior and medial-lateral radii of curvature (C_{AP} and C_{ML}) were measured as the perpendicular distances between the centroid and tibial axis in the anterior-posterior and

medial-lateral directions, respectively. Positive values for C_{AP} and C_{ML} represented anterior and medial convexities, respectively (Main et al., 2010).

2.6 Characterization of bone tissue composition by Fourier transform infrared (FTIR) imaging

Tibiae from 12 week-old LC and *Gorab*^{Prx1} mice (n=5/genotype) were dissected, dehydrated in ascending grades of ethanol, embedded in methyl methacrylate, and cut at the mid-sagittal plane with a microtome (Leica SM2500S, Germany) into 2 μm thick sections. The prepared undecalcified tibial sections were mounted on barium fluoride infrared windows for FTIR imaging (Perkin Elmer Spotlight Imaging System, MA). FTIR imaging was performed at the proximal metaphysis and mid-diaphysis of the tibia to remain consistent with the microCT regions of interest. Due to restrictions related to field of view, only the posterior side of these two regions was analyzed. The regions were scanned using a spectral resolution of 4 cm^{-1} and a spatial resolution of 6.25 μm . FTIR bone parameters calculated were (Boskey and Pleshko Camacho, 2007): mineral/matrix ratio (area of 916–1180 cm^{-1} /1590–1712 cm^{-1}); carbonate/mineral ratio (area of 852–890 cm^{-1} /916–1180 cm^{-1}); collagen maturity (peak intensity ratio of 1660 cm^{-1} /1690 cm^{-1}); crystallinity (peak intensity ratio of 1020 cm^{-1} /1030 cm^{-1}); acid phosphate content (peak height 1096 cm^{-1} /1128 cm^{-1}).

2.7 Whole-bone mechanical properties determined by three-point bending tests

Tibiae from 12 week-old LC and *Gorab*^{Prx1} mice (n=7–11/genotype) were tested to failure in three-point bending using a servohydraulic testing system (Testbench ElectroForce LM1, TA Instruments, MA) with a 25 lbs load cell (MLP 25, Transducer Techniques, CA) at a deflection rate of 0.1 mm/second. An 8.5 mm span was used for all tests. The load was applied to the anterior surface of the tibia midshaft. Load and displacement data were simultaneously collected at 20 Hz. The following parameters were reported as recommended by Jepsen et al. (Jepsen et al., 2015): maximum load (N), stiffness (N/mm), work-to-fracture (Nmm) and post-yield displacement (mm).

2.8 Data analysis

Differences in tibial morphology, bone composition, tissue-level strain and whole-bone mechanical properties between LC and *Gorab*^{Prx1} mice were tested by unpaired *t*-tests (SAS 9.4, SAS Institute, Inc, NC) to determine the effect of genotype on these outcome parameters. All data are presented as mean \pm SD. Statistical significance was set as $p < 0.05$. We also performed additional adjustments on microCT-measured bone size parameters as well as three-point bending parameters to account for body weight. The adjustments were performed using the linear regression as recommended by Jepsen et al. (Jepsen et al., 2015). The bones used for microCT, three-point bending, FTIR and strain gauge measure were all from different groups of mice. The bones used for strain gauge measures were also used for FE modeling and whole-bone morphology characterization.

3. Results

3.1 Gorab deficiency alters cross-sectional geometry of the tibia

At 10 week of age, *Gorab*^{Ptx1} and LC mice weighed 17.9±1.2 g and 23.3±1.7 g, respectively. *Gorab*^{Ptx1} mice had smaller total area, cortical area and cortical thickness, as examined at the midshaft and metaphyseal regions of the tibia, compared to LC (Fig. 2; Table 1). Compared to LC tibiae, maximum and minimum moments of inertia were decreased in *Gorab*^{Ptx1} tibiae at both the midshaft and metaphyseal regions (Fig. 2; Table 1). Interestingly, the cortical tissue mineral density (TMD) was not different between the *Gorab*^{Ptx1} and LC tibiae in the midshaft but 2% lower in *Gorab*^{Ptx1} bone for the metaphyseal region (Fig. 2; Table 1). For metaphyseal cancellous bone, *Gorab*^{Ptx1} tibiae had decreased trabecular bone volume fraction and trabecular number compared with LC tibiae (Table 1). There was a 10% increase in TMD of the metaphyseal cancellous bone of the *Gorab*^{Ptx1} tibia (Table 1). After body weight adjustment, only minimum moment of inertia of the midshaft cortical bone was affected, suggesting that the body weight difference may not explain the difference in bone size between LC and *Gorab*^{Ptx1} mice, but rather is likely attributed to the genetic perturbation.

3.2 Gorab deficiency alters cortical bone composition

In the posterior metaphyseal cortical region, the mineral/matrix ratio in *Gorab*^{Ptx1} tibiae was 36% less than LC tibiae (Fig. 3). Deficiency of *Gorab* did not affect carbonate/mineral ratio and collagen maturity (Fig. 3). There was a slight, but statistically significant decrease in crystallinity (2%) in the *Gorab*^{Ptx1} tibiae compared to the LC tibiae. Tibial acid phosphate substitution was 27% greater in *Gorab*^{Ptx1} than in LC. In the mid-diaphyseal cortical region, only acid phosphate substitution was significantly affected by *Gorab* deficiency, with the *Gorab*^{Ptx1} tibiae having 12% greater acid phosphate relative to LC (Table 2).

3.3 Gorab deficiency leads to increased anterior convex curvature

Gorab^{Ptx1} tibiae were 21% shorter than LC at the age of 10 weeks (*Gorab*^{Ptx1}: 13.5±0.9 mm; LC: 17.1±0.6 mm; p<0.001). *Gorab*^{Ptx1} tibiae had a greater anterior convex curvature compared to LC tibiae while the medial-lateral curvatures were generally similar (Fig. 4). For LC tibiae, the largest anterior-posterior convexity ($C_{AP}=1.10\pm0.03$ mm) appeared at the proximal/middle diaphysis (~35% of the tibial length from the proximal end) while this location was shifted to the mid-diaphysis of the tibia (~50% of the tibial length) for *Gorab*^{Ptx1} tibiae (Fig. 4).

3.4 Tissue-level strains are increased in tibiae from Gorab deficient compared to LC mice

The mean longitudinal strains measured at the gauge site, located on the medial surface of the tibial midshaft under -5 N loads were 543±196 µε and 1147±594 µε for LC and *Gorab*^{Ptx1} mice, respectively. The axial rigidity for LC and *Gorab*^{Ptx1} tibiae were 0.0092±0.0033 N/µε and 0.0044±0.0023 N/µε, respectively. The FE predicted mean longitudinal strain values at the gauge site were similar to experimentally measured strains for both homogeneous (LC: 505±49 µε; *Gorab*^{Ptx1}: 1191±42 µε) and heterogeneous models (LC: 564 µε; *Gorab*^{Ptx1}: 1068 µε).

Under the applied load of -5 N, the tissue-level strains throughout the entire tibia were generally higher for *Gorab*^{Prx1} than LC mice (Figs. 5 and 6A). At 25% tibial length, the maximum and minimum principal strains for *Gorab*^{Prx1} were 88% and 83% higher than LC. At 50% tibial length, the maximum and minimum principal strains for *Gorab*^{Prx1} were 127% and 73% higher than LC. At 75% tibial length, the differences in maximum or minimum principal strains between *Gorab*^{Prx1} and LC (301% or 117%) were more pronounced relative to the proximal or middle cross-sections (Figs. 5 and 6A). Tissue heterogeneity did not affect the general strain distribution along the tibia for either LC or *Gorab*^{Prx1} mice, with the exception of the proximal tibia (Fig. 6B). In the proximal metaphysis (~ 5 – 20% of bone length) of the homogeneous models, the mean maximum and minimum principal strains in *Gorab*^{Prx1} tibiae ($377 \pm 32 \mu\epsilon$ and $-558 \pm 47 \mu\epsilon$) were 54% and 42% higher than those of LC tibiae ($244 \pm 26 \mu\epsilon$ and $-395 \pm 50 \mu\epsilon$) (Figs. 6B and 7). In the proximal metaphysis of the heterogeneous models, the mean maximum and minimum principal strains in *Gorab*^{Prx1} tibiae ($757 \mu\epsilon$ and $-913 \mu\epsilon$) were 110% and 61% higher than those of LC tibiae ($361 \mu\epsilon$ and $-569 \mu\epsilon$) (Figs. 6B and 7).

3.5 Gorab deficiency compromises whole-bone mechanical properties

Tibiae from *Gorab*^{Prx1} were weaker and more brittle than tibiae from LC (Table 3). The maximum load and stiffness of *Gorab*^{Prx1} tibiae were 46% and 55% less than LC tibiae, respectively. Work-to-fracture was reduced by 61% in *Gorab*^{Prx1} compared with LC tibiae. Tibiae from *Gorab*^{Prx1} had post-yield displacement that was 47% less than tibiae from LC. None of the outcomes were affected by body-weight adjustments (Table 3).

4. Discussion

The current study focused on characterizing morphological, material and mechanical behavior of tibiae from *Gorab*^{Prx1} mice. This conditional knockout mouse had an increased anterior convexity and decreased cortical cross-sectional area, cortical thickness and moments of inertia, compared to LC tibiae. Three-point bending demonstrated whole-bone strength, stiffness and work-to-fracture of *Gorab*^{Prx1} tibiae were less than those of LC. Tibiae from *Gorab*^{Prx1} mice also appeared to be more brittle compared with LC. Tissue compositional measurements showed a decrease in mineral/matrix ratio and an increase in acid phosphate substitution in the mineral particles in the posterior metaphyseal cortex of the *Gorab*^{Prx1} tibiae, suggesting a delay in tissue mineralization. FE analysis predicted increased tissue-level strains within the *Gorab*^{Prx1} tibiae relative to LC tibiae when subjected to axial compressive loads of the same magnitude. Overall, the strain distribution along the entire tibia was similar when using homogeneous or heterogeneous material properties in the FE models although a larger difference was found in the proximal metaphysis (Figs. 6B and 7). Furthermore, we saw that the differences between the homogenous and the heterogeneous FE models in the proximal metaphyseal region were more pronounced for the *Gorab*^{Prx1} model than for the LC. These results are in line with our previous findings in C57BL/6 mice showing that assignment of homogeneous or heterogeneous material properties to the FE model does not affect the general strain distribution along the tibia, with the exception of the proximal metaphysis (Razi et al., 2015; Yang et al., 2014).

The skeletal phenotypic features observed in *Gorab*^{Prx1} tibiae are generally consistent with clinical reports on GO patients (Al-Gazali et al., 2001; Hennies et al., 2008; Hunter, 1988; Hunter et al., 1978; Lisker et al., 1979; Nanda et al., 2008; Rajab et al., 2008), who have short stature and bowed long bones (tibia and femur) and often experience bone fractures (Rajab et al., 2008). Our current results from tibial morphological measures are in agreement with previous observations of Steiner et al. 2015 (Steiner et al., 2015) showing that *Gorab* deficiency leads to a retardation of long bone growth and a dramatic reduction in trabecular and cortical bone volumes. Our three-point bending tests showed that *Gorab*^{Prx1} bones were much weaker and more brittle, suggesting that *Gorab*^{Prx1} bones are more fragile and therefore may be more susceptible to fractures than LC. This is consistent with a previous report (Steiner et al., 2015) showing that nearly all *Gorab*^{Prx1} mice in their study experienced spontaneous fractures. We observed that collagen maturity was not affected by *Gorab* deficiency, but we did observe a delay in mineralization for *Gorab* deficient bones. The delayed mineralization is supported by preliminary data by Steiner et al. showing that *Gorab* deficiency may lead to an abnormal modification of extracellular matrix proteins.

Some of the striking alterations in morphology we observed with *Gorab* deficiency are consistent with chronologically or accelerated aging mice. Studies in C57BL/6 mice show tibial cortical area and thickness increase between 6 weeks and 6 months of age and then decline up to 22 months of age (Galea et al., 2015; Halloran et al., 2002; Patel et al., 2014). The anterior-posterior curvature of the tibiae of female C57BL/6 mice increases with aging, similar to what we have observed in the female premature aged *Gorab*^{Prx1} mice (Galea et al., 2015; Patel et al., 2014; Razi et al., 2015). Some morphological characteristics of senescence-accelerated mouse strain P6 (SAMP6) long bones overlap with our mouse model (Matsushita et al., 1986; Silva et al., 2002; Silva et al., 2004; Takeda et al., 1981). Relative to LC, we measured largely decreased maximum load, stiffness and work-to-fracture and increased brittleness in *Gorab*^{Prx1} tibiae. The reduction of whole-bone mechanical properties in *Gorab*^{Prx1} tibiae is related with decreased cross-sectional area and moment of inertia. The alterations in these measured whole-tibia strength and work-to-fracture are consistent with reports of age-related changes in human bones (Courtney et al., 1995; Martin and Atkinson, 1977), C57BL/6 mice (Almeida et al., 2007; Ferguson et al., 2003; Hamrick et al., 2006) and SAMP6 mice (Silva et al., 2002; Silva et al., 2004).

The curvatures in the long bones augment rather than diminish stress/strain generated in bone (Biewener, 1983, 1991). Although a curved bone is not the most efficient structure to obtain a tradeoff between the opposing objectives of stiffness and lightness (Currey, 2014), it has the benefit of providing loading predictability, i.e. control of the direction of load-induced bending (Bertram and Biewener, 1988). We found that *Gorab*^{Prx1} mice had increased tibial curvature, as is the case in chronologically aged mice (Galea et al., 2015; Patel et al., 2014; Razi et al., 2015). Although local strain history is a major determinant of the tissue response, it is not known to what extent the bone's curvature of *Gorab*^{Prx1} mice is genetically driven or a result of alteration of external mechanical environments and bone tissue material properties.

The microCT-measured TMD was similar between *Gorab*^{Prx1} and LC tibiae in the midshaft but 2% lower in the metaphyseal cortex and 10% higher in the metaphyseal cancellous bone

for *Gorab*^{Prx1} tibiae. The regional differences in changes of TMD associated with *Gorab* deficiency could partly be attributed to the different mechanical environments that the bones experience (Yang et al., 2014) or it is also possible that cancellous tissues are more sensitive to genetic perturbation of *Gorab* than cortical bone. Similar to TMD, we measured greater differences in FTIR parameters (e.g. mineral/matrix) in the proximal relative to mid-diaphyseal regions. Since a greater difference in cross-sectional area between *Gorab*^{Prx1} and LC tibiae was found in the metaphysis than the mid-diaphysis, it remains unclear if there exists any relationship between the bone geometry and tissue composition and further investigation may be warranted. The acid phosphate substitution increased in both metaphyseal and diaphyseal cortical bone for the *Gorab*^{Prx1} tibiae. These tissue compositional changes are not in line with age-related changes in human bone composition, where the mineral/matrix ratio increases and acid phosphate content decreases with chronological aging (Boskey, 2013; Gamsjaeger et al., 2014). Bone composition in *Gorab*^{Prx1} tibiae is also not consistent with what has been reported in osteogenesis imperfecta (Type VII and VIII), whereby mineral/matrix increases (Lindahl et al., 2011; Vanleene et al., 2011). Further investigations are necessary to understand the mechanism(s) responsible for the altered bone composition in *Gorab*^{Prx1} mice.

Our study has limitations. Mice cortical bone, unlike humans lacks Haversian remodeling (Jilka, 2013). However, mice models, particularly the C57BL/6 mouse strain share many characteristics of human skeletal aging such as cortical thinning, increased cortical porosity, and cancellous bone loss (Jilka, 2013). The accuracy of the three-point bending tests may have been affected by our choice of such a large load cell and choice of using the same span length for both genotypes. Also, tibiae were tested in the anterior-posterior direction with three-point bending, which may cause local buckling and violate beam theory assumption when estimating tissue mechanical properties. However, we remain confident in our general findings given the large differences we observed between LC and *Gorab*^{Prx1} bones. Lastly, outcome measures were performed on two ages, 10 and 12 week-old mice, which encompasses a time of rapid growth. Future two-week in vivo tibial loading studies are planned and thus these ages were chosen since they represent the onset and end point of those experiments.

In summary, we measured striking alterations in morphological, material, and mechanical properties associated with *Gorab* deficiency. *Gorab*^{Prx1} tibiae have increased anterior curvature, decreased cortical cross-sectional area and moments of inertia, compromised whole-bone strength, increased tissue-level strains and delayed mineralization, compared to LC tibiae. Many of these characteristics recapitulate aging-related changes in the human skeleton or in other animal models of chronological aging. These data in this conditional mouse model provide valuable insights into how changes in bone strength and composition may be affecting human patients with GO, thereby contributing to their osteoporotic phenotype.

Acknowledgments

This study was supported by the German Federal Ministry of Education and Research (TP5/DIMEOs), German Research Foundation (WI3761/4-1, CH1123/4-1, KO2891/4-1, FOR2165), National Institutes of Health (AR041325, AR046121), European Community's Seventh Framework Programme (SYBIL:602300), National

Natural Science Foundation of China (11702008), Beijing University of Technology Seed Fund for International Collaboration (015000514117514), Shriners Hospitals for Children, and Réseau de recherche en santé buccodentaire et osseuse recruitment aid program.

References

- Albiol, L., Pflanz, D., Cilla, M., Kramer, I., Kneissel, M., Duda, G., Zaslansky, P., Willie, BM., Checa, S. Sost deficiency leads to a reduction in the mechanical strains induced within the mouse tibia. Proceedings of the Orthopaedic Research Society Annual Meeting; San Diego, California. 2017.
- Al-Bughaili M, Neuhann TM, Flottmann R, Mundlos S, Spielmann M, Kornak U, Fischer-Zirnsak B. A de novo 1q23.3–q24.2 deletion combined with a GORAB missense mutation causes a distinctive phenotype with cutis laxa. *J Hum Genet.* 2017; 62:325–328. [PubMed: 27604556]
- Al-Gazali LI, Sztriha L, Skaff F, Haas D. Gerodermia osteodysplastica and wrinkly skin syndrome: are they the same? *Am J Med Genet.* 2001; 101:213–220. [PubMed: 11424136]
- Almeida M, Han L, Martin-Millan M, Plotkin LI, Stewart SA, Roberson PK, Kousteni S, O'Brien CA, Bellido T, Parfitt AM, Weinstein RS, Jilka RL, Manolagas SC. Skeletal involution by age-associated oxidative stress and its acceleration by loss of sex steroids. *The Journal of biological chemistry.* 2007; 282:27285–27297. [PubMed: 17623659]
- Bertram JE, Biewener AA. Bone curvature: sacrificing strength for load predictability? *Journal of theoretical biology.* 1988; 131:75–92. [PubMed: 3419194]
- Biewener AA. Allometry of quadrupedal locomotion: the scaling of duty factor, bone curvature and limb orientation to body size. *The Journal of experimental biology.* 1983; 105:147–171. [PubMed: 6619724]
- Biewener AA. Musculoskeletal design in relation to body size. *Journal of biomechanics.* 1991; 24(Suppl 1):19–29. [PubMed: 1791177]
- Boskey A, Pleshko Camacho N. FT-IR imaging of native and tissue-engineered bone and cartilage. *Biomaterials.* 2007; 28:2465–2478. [PubMed: 17175021]
- Boskey AL. Bone composition: relationship to bone fragility and antiosteoporotic drug effects. *Bonekey Rep.* 2013; 2:447. [PubMed: 24501681]
- Courtney AC, Wachtel EF, Myers ER, Hayes WC. Age-related reductions in the strength of the femur tested in a fall-loading configuration. *J Bone Joint Surg Am.* 1995; 77:387–395. [PubMed: 7890787]
- Currey, JD. The mechanical adaptations of bones. Princeton University Press; 2014.
- De Souza RL, Matsuura M, Eckstein F, Rawlinson SC, Lanyon LE, Pitsillides AA. Non-invasive axial loading of mouse tibiae increases cortical bone formation and modifies trabecular organization: a new model to study cortical and cancellous compartments in a single loaded element. *Bone.* 2005; 37:810–818. [PubMed: 16198164]
- Egerer J, Emmerich D, Fischer-Zirnsak B, Chan WL, Meierhofer D, Tuysuz B, Marschner K, Sauer S, Barr FA, Mundlos S, Kornak U. GORAB Missense Mutations Disrupt RAB6 and ARF5 Binding and Golgi Targeting. *J Invest Dermatol.* 2015; 135:2368–2376. [PubMed: 26000619]
- Ferguson VL, Ayers RA, Bateman TA, Simske SJ. Bone development and age-related bone loss in male C57BL/6J mice. *Bone.* 2003; 33:387–398. [PubMed: 13678781]
- Galea GL, Hannuna S, Meakin LB, Delisser PJ, Lanyon LE, Price JS. Quantification of Alterations in Cortical Bone Geometry Using Site Specificity Software in Mouse models of Aging and the Responses to Ovariectomy and Altered Loading. *Front Endocrinol (Lausanne).* 2015; 6:52. [PubMed: 25954246]
- Gamsjaeger S, Brozek W, Recker R, Klaushofer K, Paschalis EP. Transmenopausal changes in trabecular bone quality. *Journal of bone and mineral research.* 2014; 29:608–617. [PubMed: 23966337]
- Glorieux FH, Moffatt P. Osteogenesis imperfecta, an ever-expanding conundrum. *Journal of bone and mineral research.* 2013; 28:1519–1522. [PubMed: 23696068]
- Halloran BP, Ferguson VL, Simske SJ, Burghardt A, Venton LL, Majumdar S. Changes in bone structure and mass with advancing age in the male C57BL/6J mouse. *Journal of bone and mineral research.* 2002; 17:1044–1050. [PubMed: 12054159]

- Hamrick MW, Ding KH, Pennington C, Chao YJ, Wu YD, Howard B, Immel D, Borlongan C, McNeil PL, Bollag WB, Curl WW, Yu J, Isales CM. Age-related loss of muscle mass and bone strength in mice is associated with a decline in physical activity and serum leptin. *Bone*. 2006; 39:845–853. [PubMed: 16750436]
- Hennies HC, Kornak U, Zhang H, Egerer J, Zhang X, Seifert W, Kuhnisch J, Budde B, Natebus M, Brancati F, Wilcox WR, Muller D, Kaplan PB, Rajab A, Zampino G, Fodale V, Dallapiccola B, Newman W, Metcalfe K, Clayton-Smith J, Tassabehji M, Steinmann B, Barr FA, Nurnberg P, Wieacker P, Mundlos S. Geroderma osteodysplastica is caused by mutations in SCYL1BP1, a Rab-6 interacting golgin. *Nature genetics*. 2008; 40:1410–1412. [PubMed: 18997784]
- Hunter AG. Is geroderma osteodysplastica underdiagnosed? *J Med Genet*. 1988; 25:854–857. [PubMed: 3236370]
- Hunter AG, Martsolf JT, Baker CG, Reed MH. Geroderma osteodysplastica. A report of two affected families. *Hum Genet*. 1978; 40:311–324. [PubMed: 631850]
- Jepsen KJ, Silva MJ, Vashishth D, Guo XE, van der Meulen MC. Establishing biomechanical mechanisms in mouse models: practical guidelines for systematically evaluating phenotypic changes in the diaphyses of long bones. *Journal of bone and mineral research*. 2015; 30:951–966. [PubMed: 25917136]
- Jilka RL. The relevance of mouse models for investigating age-related bone loss in humans. *The journals of gerontology. Series A, Biological sciences and medical sciences*. 2013; 68:1209–1217.
- Lindahl K, Barnes AM, Fratzl-Zelman N, Whyte MP, Hefferan TE, Makareeva E, Brusel M, Yaszemski MJ, Rubin CJ, Kindmark A, Roschger P, Klaushofer K, McAlister WH, Mumm S, Leikin S, Kessler E, Boskey AL, Ljunggren O, Marini JC. COL1 C-propeptide cleavage site mutations cause high bone mass osteogenesis imperfecta. *Hum Mutat*. 2011; 32:598–609. [PubMed: 21344539]
- Lisker R, Hernandez A, Martinez-Lavin M, Mutchinick O, Armas C, Reyes P, Robles-Gil J. Geroderma osteodysplastica hereditaria: report of three affected brothers and literature review. *Am J Med Genet*. 1979; 3:389–395. [PubMed: 474638]
- Logan M, Martin JF, Nagy A, Lobe C, Olson EN, Tabin CJ. Expression of Cre Recombinase in the developing mouse limb bud driven by a Prxl enhancer. *Genesis*. 2002; 33:77–80. [PubMed: 12112875]
- Main RP, Lynch ME, van der Meulen MC. In vivo tibial stiffness is maintained by whole bone morphology and cross-sectional geometry in growing female mice. *Journal of biomechanics*. 2010; 43:2689–2694. [PubMed: 20673665]
- Martin RB, Atkinson PJ. Age and sex-related changes in the structure and strength of the human femoral shaft. *Journal of biomechanics*. 1977; 10:223–231. [PubMed: 858728]
- Matsushita M, Tsuboyama T, Kasai R, Okumura H, Yamamuro T, Higuchi K, Higuchi K, Kohno A, Yonezu T, Utani A, et al. Age-related changes in bone mass in the senescence-accelerated mouse (SAM). SAM-R/3 and SAM-P/6 as new murine models for senile osteoporosis. *Am J Pathol*. 1986; 125:276–283. [PubMed: 3789087]
- Nanda A, Alsaleh QA, Al-Sabah H, Marzouk EE, Salam AM, Nanda M, Anim JT. Geroderma osteodysplastica/wrinkly skin syndrome: report of three patients and brief review of the literature. *Pediatr Dermatol*. 2008; 25:66–71. [PubMed: 18304158]
- Nistala H, Lee-Arteaga S, Carta L, Cook JR, Smaldone S, Siciliano G, Rifkin AN, Dietz HC, Rifkin DB, Ramirez F. Differential effects of alendronate and losartan therapy on osteopenia and aortic aneurysm in mice with severe Marfan syndrome. *Hum Mol Genet*. 2010; 19:4790–4798. [PubMed: 20871099]
- Patel TK, Brodt MD, Silva MJ. Experimental and finite element analysis of strains induced by axial tibial compression in young-adult and old female C57Bl/6 mice. *Journal of biomechanics*. 2014; 47:451–457. [PubMed: 24268312]
- Rajab A, Kornak U, Budde BS, Hoffmann K, Jaeken J, Nurnberg P, Mundlos S. Geroderma osteodysplastica hereditaria and wrinkly skin syndrome in 22 patients from Oman. *Am J Med Genet A*. 2008; 146A:965–976. [PubMed: 18348262]

- Razi H, Birkhold AI, Zaslansky P, Weinkamer R, Duda GN, Willie BM, Checa S. Skeletal maturity leads to a reduction in the strain magnitudes induced within the bone: a murine tibia study. *Acta biomaterialia*. 2015; 13:301–310. [PubMed: 25463494]
- Silva MJ, Brodt MD, Ettner SL. Long bones from the senescence accelerated mouse SAMP6 have increased size but reduced whole-bone strength and resistance to fracture. *Journal of bone and mineral research*. 2002; 17:1597–1603. [PubMed: 12211429]
- Silva MJ, Brodt MD, Fan Z, Rho JY. Nanoindentation and whole-bone bending estimates of material properties in bones from the senescence accelerated mouse SAMP6. *Journal of biomechanics*. 2004; 37:1639–1646. [PubMed: 15388305]
- Steiner MCH, Schinke T, Eppendorf H, Amling M, Chan D, Mundlos S, Kornak U. Dysregulated TGF- β signaling and oxidative DNA damage as the cause for osteoporosis in the progeroid disorder gerodermia osteodysplastica. *Journal of bone and mineral research*. 2015; 30(Suppl 1)
- Sugiyama T, Meakin LB, Browne WJ, Galea GL, Price JS, Lanyon LE. Bones' adaptive response to mechanical loading is essentially linear between the low strains associated with disuse and the high strains associated with the lamellar/woven bone transition. *Journal of bone and mineral research*. 2012; 27:1784–1793. [PubMed: 22431329]
- Takeda T, Hosokawa M, Takeshita S, Irino M, Higuchi K, Matsushita T, Tomita Y, Yasuhira K, Hamamoto H, Shimizu K, Ishii M, Yamamuro T. A new murine model of accelerated senescence. *Mech Ageing Dev*. 1981; 17:183–194. [PubMed: 7311623]
- Vanleene M, Saldanha Z, Cloyd KL, Jell G, Bou-Gharios G, Bassett JH, Williams GR, Fisk NM, Oyen ML, Stevens MM, Guillot PV, Shefelbine SJ. Transplantation of human fetal blood stem cells in the osteogenesis imperfecta mouse leads to improvement in multiscale tissue properties. *Blood*. 2011; 117:1053–1060. [PubMed: 21088133]
- Willie BM, Birkhold AI, Razi H, Thiele T, Aido M, Kruck B, Schill A, Checa S, Main RP, Duda GN. Diminished response to in vivo mechanical loading in trabecular and not cortical bone in adulthood of female C57Bl/6 mice coincides with a reduction in deformation to load. *Bone*. 2013; 55:335–346. [PubMed: 23643681]
- Yang H, Butz KD, Duffy D, Niebur GL, Nauman EA, Main RP. Characterization of cancellous and cortical bone strain in the in vivo mouse tibial loading model using microCT-based finite element analysis. *Bone*. 2014; 66:131–139. [PubMed: 24925445]
- Yang H, Embry RE, Main RP. Effects of loading duration and short rest insertion on cancellous and cortical bone adaptation in the mouse tibia. *PloS one*. 2017; 12:e0169519. [PubMed: 28076363]

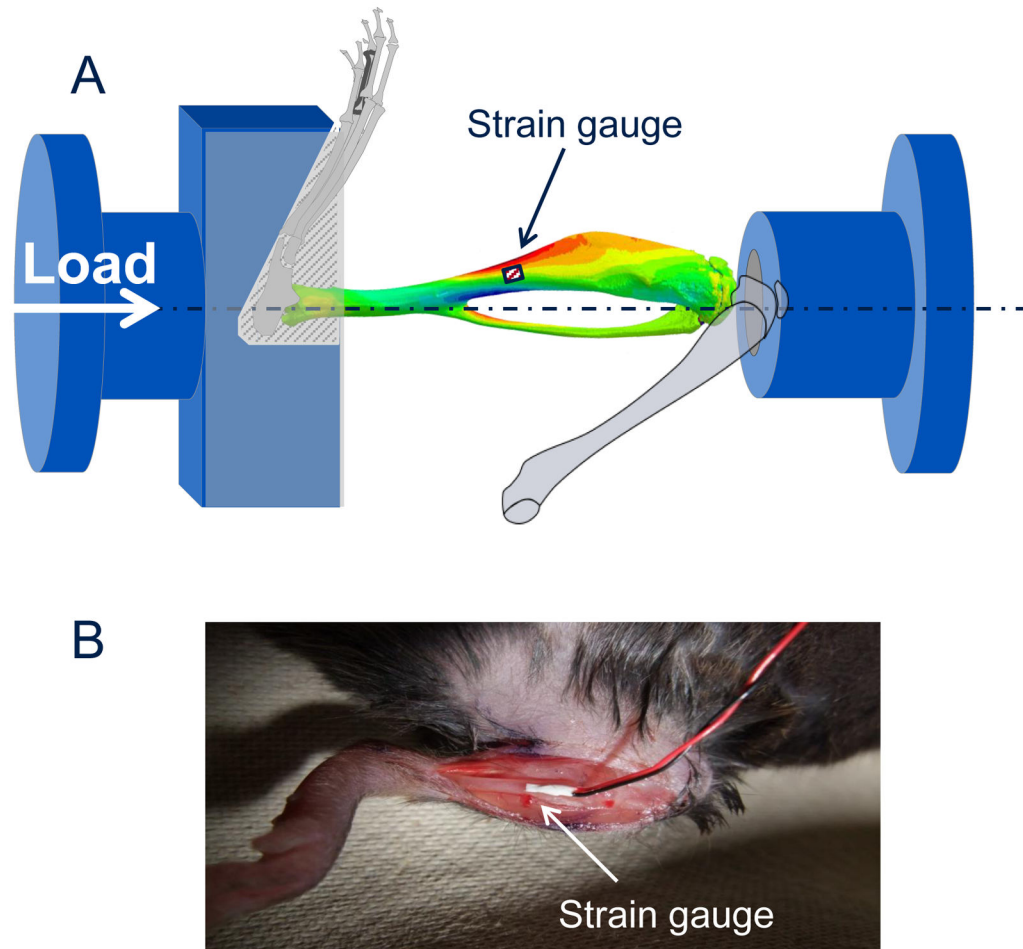


Fig. 1. (A) Schematic showing the experimental configuration for *in vivo* strain gauging and compressive loading of the mouse tibia. (B) A strain gauged tibia showing the position of the gauge *in vivo*.

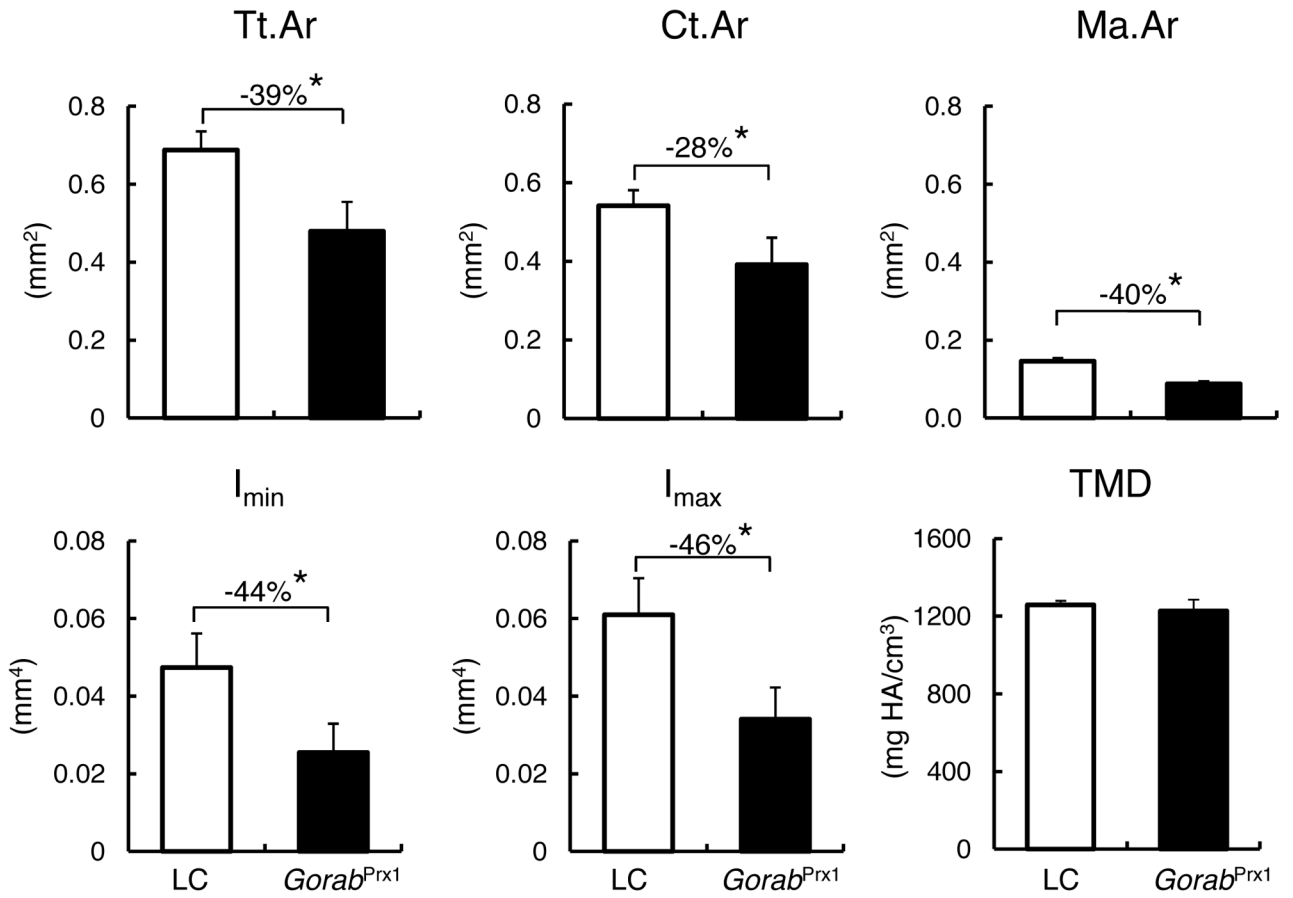


Fig. 2. Differences in cross-sectional geometry and tissue mineral density (TMD) of the midshaft of the tibia (5% of total tibial length) between LC and *Gorab^{Prx1}* mice, measured by microCT.
* $p < 0.05$ by unpaired *t*-test.

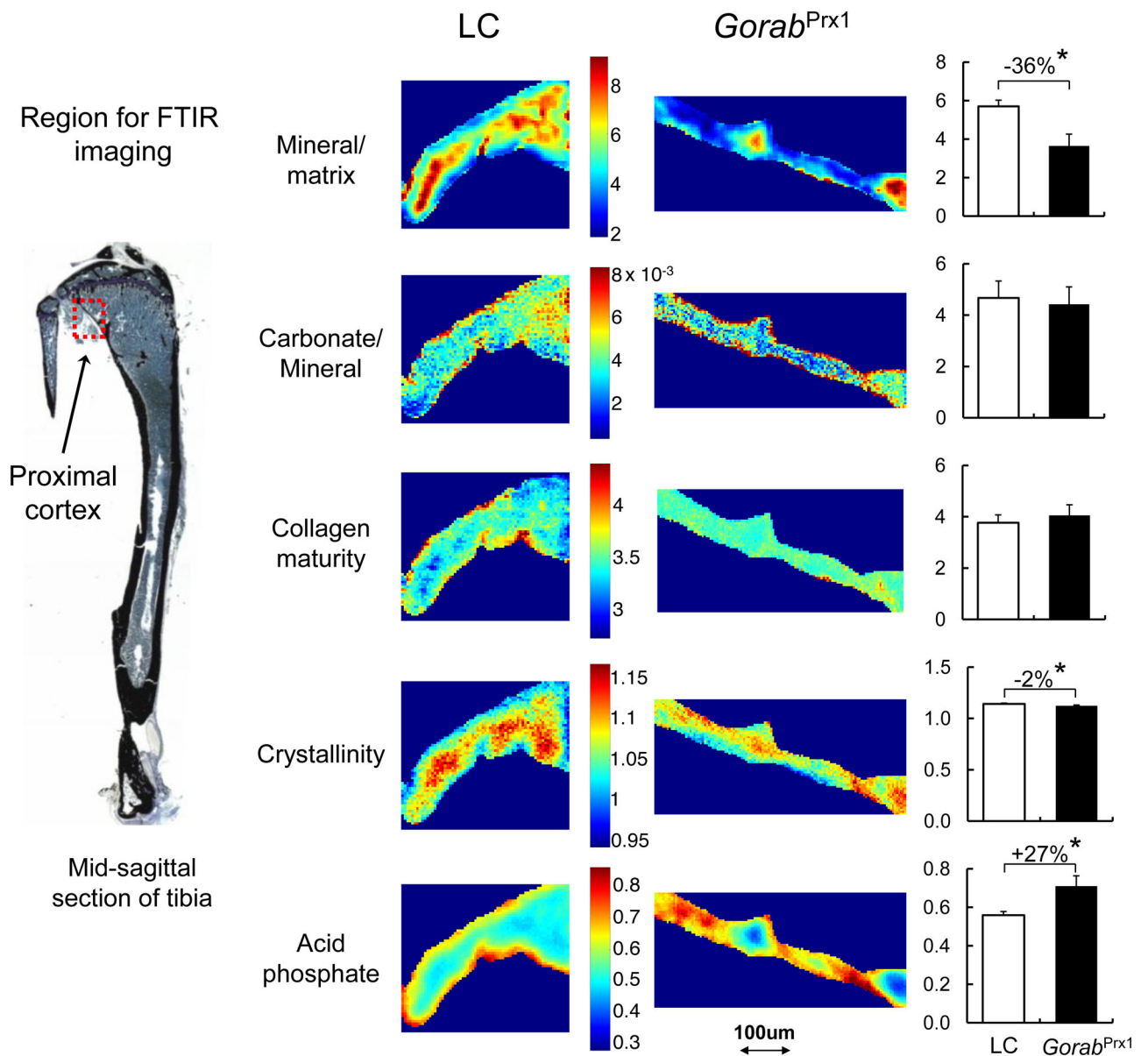


Fig. 3. Representative FTIR images of the cortical bone from the proximal posterior metaphyseal region of the LC and *Gorab^{Prx1}* tibiae. The color scale for all images for an indicated variable (mineral/matrix ratio, carbonate/mineral ratio, collagen maturity, crystallinity and acid phosphate) is shown besides the images for that group. Quantitative data show that *Gorab^{Prx1}* tibiae have decreased mineral/matrix ratio (-36%) and increased acid phosphate (+27%). * $p < 0.05$ by unpaired *t*-test.

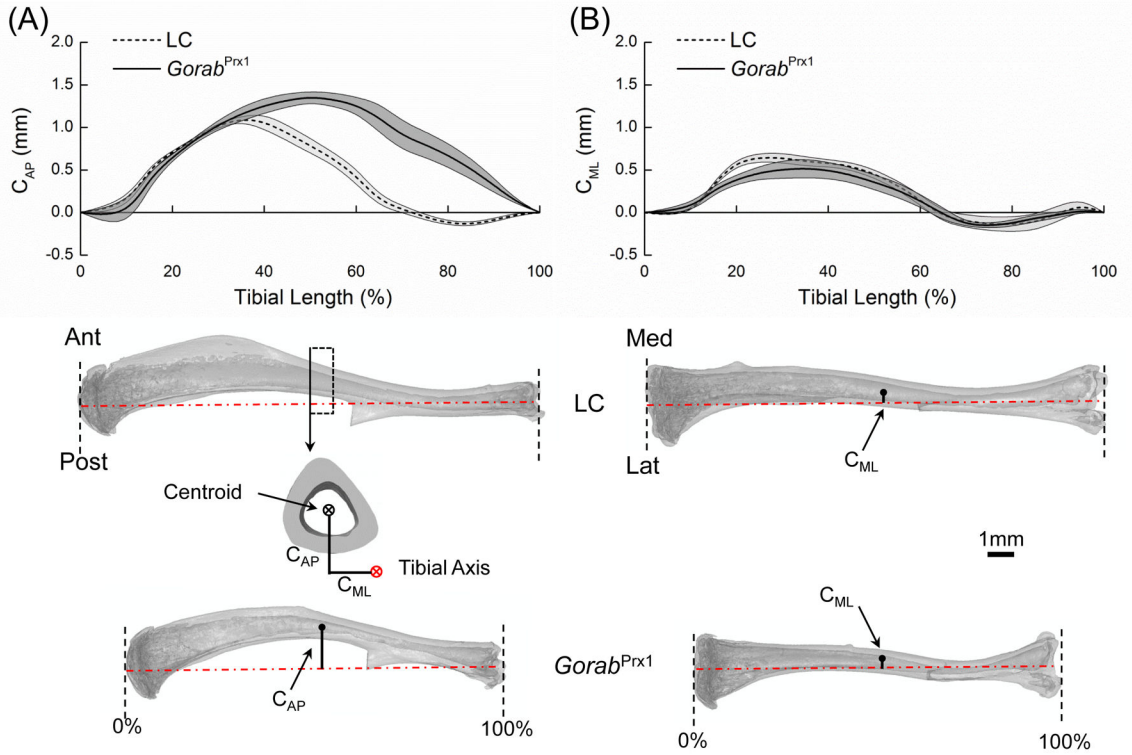


Fig. 4. Comparison of whole-bone curvatures between LC and *Gorab^{Prx1}* tibiae. The anterior-posterior and medial-lateral longitudinal bone curvatures (C_{AP} and C_{ML}) were measured as the perpendicular distances from the centroid of a tibial cross-section to the tibial axis in the anterior-posterior and medial-lateral directions, respectively. Tibial axis was determined by the centroids of the proximal and distal sections.

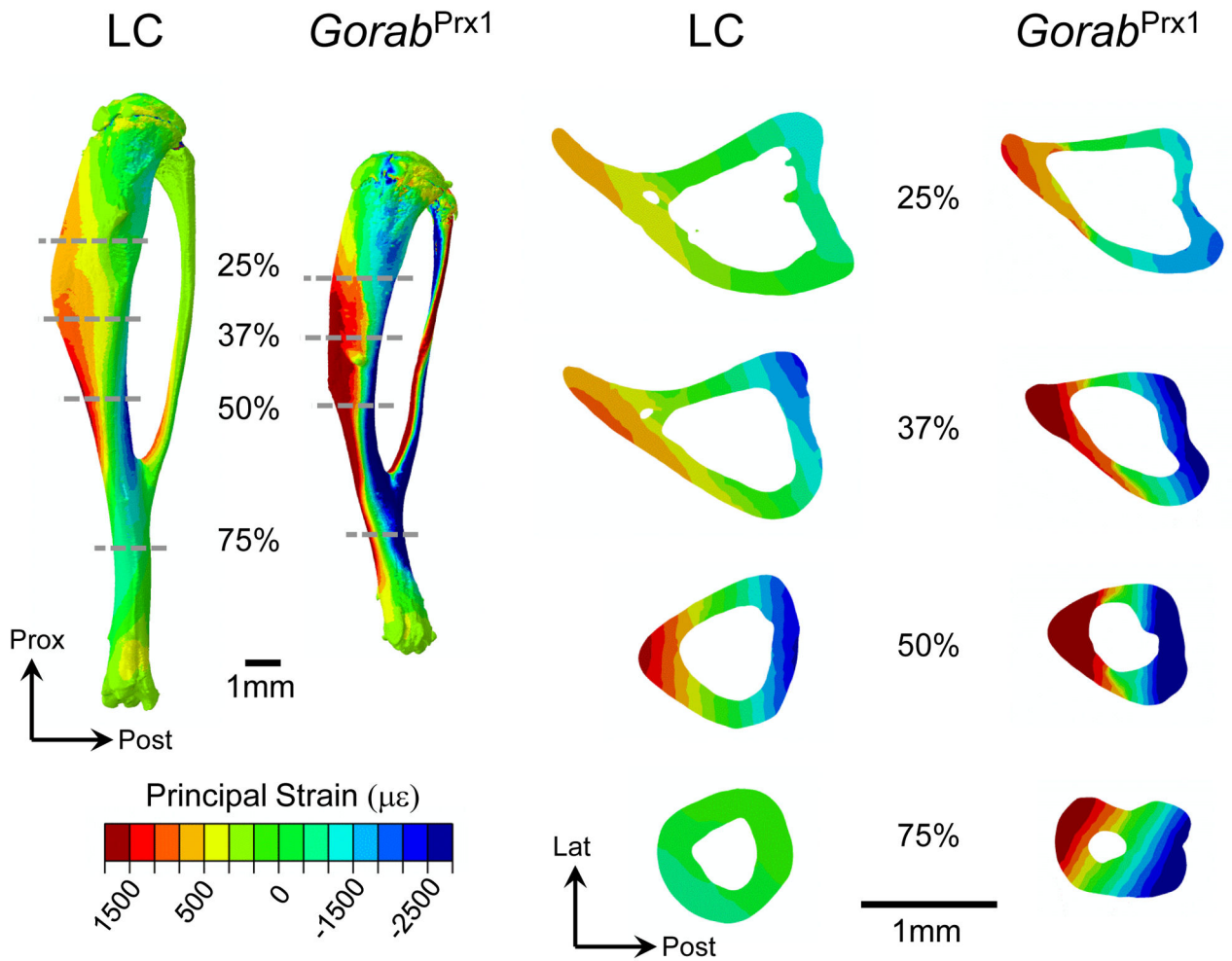


Fig. 5. Computationally predicted principal strain distributions throughout the entire tibia and at multiple representative cross-sections (25%, 37%, 50% and 75% relative to the proximal end) for the LC and *Gorab*^{Prx1} limbs loaded with 5 N in uniaxial compression *in vivo*. Red and blue indicate tensile and compressive strains, respectively. Strain gauge was attached on the medial surface of the tibial midshaft to measure the longitudinal strain there experimentally.

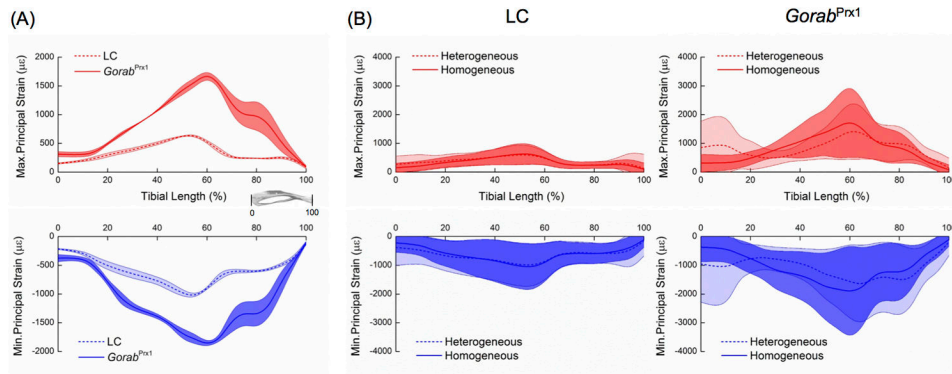


Fig. 6. (A) Variations of the maximum and minimum principal strains along the tibial length for LC and *Gorab*^{Prx1} tibiae loaded with 5 N in compression. The lines and areas represent mean \pm standard deviation of the average (maximum or minimum principal) strain value in each cross-section of the tibia (n=3/genotype); (B) Comparison of strain distributions along the tibial length (proximal end: 0%; distal end: 100%) between homogeneous and heterogeneous FE models for LC and *Gorab*^{Prx1} tibiae subjected to compression loading of 5 N (n=1/genotype). The lines and areas represent mean \pm standard deviation of the maximum or minimum principal strain values in each cross-section of the tibia.

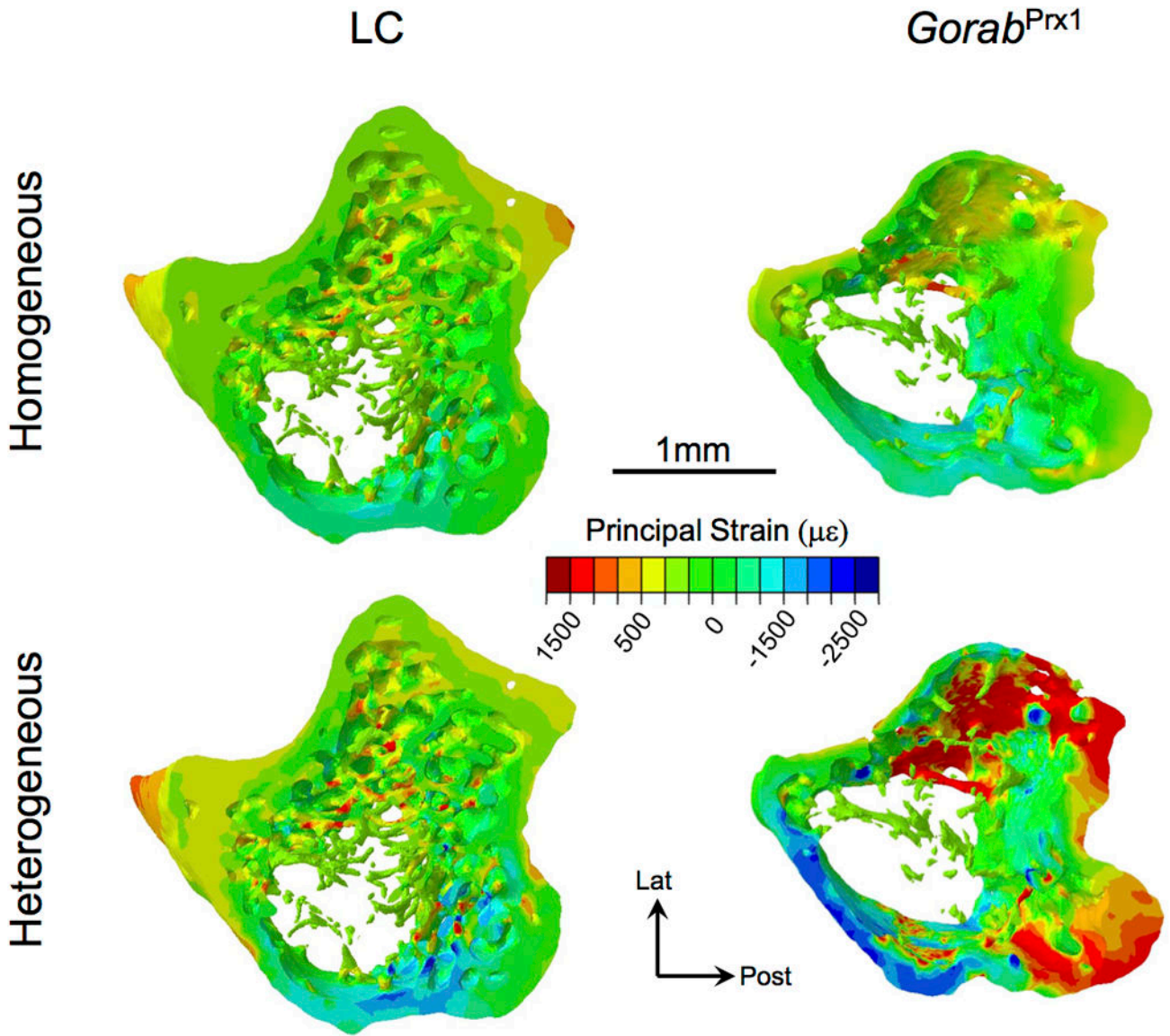


Fig. 7. Strain distributions in the proximal metaphysis (starting 100 µm below the distal-most point of the growth plate and extending distally 10% of the tibial length) of both homogeneous and heterogeneous FE models of the LC and *Gorab*^{Prx1} tibiae. Both tensile (+) and compressive (-) strains are shown.

Table 1

MicroCT-measured geometric or structural parameters for the proximal metaphyseal cortical and cancellous bone of the LC and *Gorab*^{Prx1} tibiae, located just below the growth plate extending 10% of the tibial length distally.

Parameters	LC	<i>Gorab</i> ^{Prx1}	Difference (%)
Metaphyseal cortical bone			
Ct.Ar (mm ²)	0.890 ± 0.090	0.358 ± 0.078 <i>b</i>	-60
Tt.Ar (mm ²)	1.413 ± 0.120	1.020 ± 0.180 <i>b</i>	-28
Ma.Ar (mm ²)	0.523 ± 0.090	0.659 ± 0.150	26
Ct.Th (mm)	0.111 ± 0.015	0.053 ± 0.008 <i>b</i>	-52
I _{max} (mm ⁴)	0.375 ± 0.072	0.209 ± 0.035 <i>b</i>	-44
I _{min} (mm ⁴)	0.256 ± 0.046	0.076 ± 0.028 <i>b</i>	-70
Ct.TMD (mgHA/ccm)	1075 ± 20	1052 ± 17 <i>a</i>	-2
Metaphyseal cancellous bone			
BV/TV (%)	9.6 ± 3.0	4.7 ± 1.7 <i>b</i>	-50
Tb.Th (μm)	46 ± 4	45 ± 5	-3
Tb.N (1/mm)	4.2 ± 0.5	3.6 ± 0.5 <i>a</i>	-14
Tb.Sp (μm)	244 ± 29	281 ± 44	15
Tb.TMD (mgHA/ccm)	791 ± 31	870 ± 32 <i>b</i>	10

Data are presented as mean ± SD.

Differences are calculated as $(Gorab^{Prx1} - LC) / LC \times 100$.

a p < 0.05 relative to LC.

b p < 0.001 relative to LC.

Table 2

FTIR-measured compositional parameters for cortical bone at the posterior midshaft of the tibiae from 12 week-old LC and *Gorab*^{Prx1} mice.

Parameters	LC	<i>Gorab</i> ^{Prx1}	Difference (%)
Mineral/matrix	6.58 ± 0.31	5.97 ± 0.59	-9
Carbonate/mineral ×10 ³	5.4 ± 0.4	5.4 ± 0.5	0
Collagen maturity	3.54 ± 0.21	3.85 ± 0.42	9
Crystallinity	1.16 ± 0.02	1.15 ± 0.01	-1
Acid phosphate	0.46 ± 0.02	0.51 ± 0.02 ^a	12

Data are presented as mean ± SD.

Differences are calculated as $(Gorab^{Prx1}-LC)/LC \times 100$.

^ap<0.05 relative to LC.

Whole-bone mechanical properties of 12 week-old LC and *Gorab^{Pxx1}* tibiae, measured by three-point bending testing.

Table 3

Parameters	Unadjusted				Body weight-adjusted			
	LC	<i>Gorab^{Pxx1}</i>	Diff (%)	LC	LC	<i>Gorab^{Pxx1}</i>	Diff (%)	Diff (%)
Max load (N)	13.00 ± 1.77	6.97 ± 2.71 ^a	-46	14.44 ± 1.57	8.73 ± 1.97 ^a	-40		
Stiffness (N/mm)	148.1 ± 21.5	67.2 ± 32.1 ^a	-55	153.1 ± 21.3	85.0 ± 26.0 ^a	-45		
Work-to-fracture (Nmm)	12.50 ± 3.82	4.93 ± 4.41 ^a	-61	18.22 ± 2.02	7.24 ± 3.68 ^a	-60		
Post-yield displacement (mm)	0.48 ± 0.22	0.25 ± 0.23 ^a	-47	0.71 ± 0.18	0.33 ± 0.21 ^a	-54		

Data are presented as mean ± SD.

Differences are calculated as (*Gorab^{Pxx1}*-LC)/LC×100.

^ap<0.05 relative to LC.